Materials Science & Engineering B 229 (2018) 218–226

Contents lists available at ScienceDirect

Materials Science & Engineering B

journal homepage: www.elsevier.com/locate/mseb

Photocatalytic evaluation of the magnetic core@shell system (Co,Mn)Fe_2O_4@TiO_2 obtained by the modified Pechini method

A.M. Neris[a], W.H. Schreiner[b], C. Salvador[c], U.C. Silva[d], C. Chesman[d], E. Longo[e], I.M.G. Santos[a,*]

[a] Núcleo de Pesquisa e Extensão: Laboratório de Combustíveis e Materiais, Universidade Federal da Paraíba, João Pessoa, PB, Brazil
[b] Laboratório de Superfícies e Interfaces – Universidade Federal do Paraná, Curitiba, PR, Brazil
[c] Departamento de Física, Universidade Federal da Paraíba, João Pessoa, PB, Brazil
[d] Departamento de Física, Universidade Federal do Rio Grande do Norte, Natal, RN, Brazil
[e] Laboratório Interdisciplinar de Eletroquímica e Cerâmica/Centro para o Desenvolvimento de Materiais Funcionais, Universidade Estadual Paulista Julio de Mesquita Filho, Araraquara, SP, Brazil

ARTICLE INFO

Keywords:
Core-shell
Anatase
(Co,Mn)Fe_2O_4@TiO_2
Photocatalysis

ABSTRACT

TiO_2 is a highly active photocatalyst, sometimes obtained with nanometric particle size, which improves its behavior but makes its removal from aqueous media more difficult. To avoid this drawback, this work aims to obtain a photocatalyst easily removable from aqueous media using magnetism. The core@shell system (Co,Mn)Fe_2O_4@TiO_2 was prepared by adding commercial (Co,Mn)Fe_2O_4 nanoparticles to the titanium polymeric resin synthesized by the modified Pechini method. Optimization of photocatalyst properties was achieved by variation of the TiO_2:ferrite ratio, synthesis temperature and time, followed by their evaluation in photodegradation of an azo dye. The highest efficiency was attained when anatase was the major crystalline phase, whereas TiO_2:ferrite ratio was limited to 90% to retain the magnetic properties, which enabled its removal from aqueous media using simple magnets. The system (Co,Mn)Fe_2O_4@TiO_2, synthesized with 90% TiO_2 and calcined at 500 °C for 8 h, presented a discoloration of 76.3% after 16 h of exposure to UV light.

1. Introduction

Titanium dioxide is a semiconductor material widely used in heterogeneous photocatalysis due to its high photochemical reactivity, stability in aqueous systems and low environmental toxicity [1–4]. TiO_2 usually crystallizes as anatase, rutile or brookite, whereas rutile is thermodynamically most stable, anatase is the most stable structure in nanometric scale and highly explored in photocatalysis [5–8]. Many studies describe excellent results with the use of TiO_2 as a photocatalyst for different applications, such as treatment of organic residues [9], including dyes [10,11], pesticides [12] and microorganisms [13], with the possibility of using natural and artificial energy sources [14–16]. For instance, the commercial P25 TiO_2 (Evonik) is considered a reference for comparison with new photocatalysts, due to excellent results obtained with this material [17,18].

However, even for a heterogeneous process, removal of nanometric photocatalysts from aqueous media may present difficulties, whereas its combination with magnetic materials can make separation processes much easier [19]. Use of a core@shell system, with a nucleus composed of nanometric material covered with TiO_2, favors catalyst separation from an aqueous media and keeps the photocatalytic properties and material dispersion characteristics of nanometric materials [20,21].

Considering inorganic core@shell systems, the sol-gel method and the hydrothermal/solvothermal method have been the most explored techniques as shown elsewhere [22,23]. For instance, Xin et al. reports the synthesis of the Fe_3O_4@TiO_2 core@shell system by the solvothermal method, with good magnetic properties at room temperature and good photocatalytic activity for degradation of Rhodamine B dye (RhB) in solution [24]. Choi et al. [25] evaluated the Ag-doping of this same material and reported improved photocatalytic efficiency for RhB degradation and for trichlorophenol oxidation under visible light, as well as for its reuse. The reuse of a core-shell photocatalyst was also determined by Zheng et al. [26], who evaluated the photodegradation of methylene blue by Fe_3O_4@TiO_2 obtained by the liquid phase deposition (LPD) method, using visible irradiation with a high efficiency. Habila et al. [20] reported the high photocatalytic efficiency of the core@shell system containing a magnetic core and multiple layers, forming the Fe_3O_4@SiO_2@TiO_2 system for decomposition of tartrazine and the yellow twilight in aqueous solution under UV radiation. Harraz et al. [27] synthesized titania-silica/cobalt ferrite nanocomposite with a surface area higher than 400 $m^2 g^{-1}$ by the sol-gel method for methylene blue degradation, with a high photocatalytic efficiency. The

* Corresponding author.
E-mail address: ieda@quimica.ufpb.br (I.M.G. Santos).

https://doi.org/10.1016/j.mseb.2017.12.029
Received 15 August 2017; Received in revised form 16 December 2017; Accepted 27 December 2017
Available online 09 January 2018

hydrothermal method was used by Wilson et al. [28] to obtain the system $CoFe_2O_4$@ZnO using carbon nanospheres derived from glucose as a template. The authors reported a relationship between ZnO shell thickness and photocatalytic efficiency in methylene blue degradation in aqueous solution under UV radiation. Wu et al. [29] synthesized magnetic iron oxides/TiO_2 hybrid nanoparticles by the solvothermal method and obtained a large degree of photocatalytic degradation of methylene blue. In addition to other core@shell systems with magnetic cores, the use of structures containing Ag [30,31] or Cu [32] stands out for photocatalytic applications.

The Pechini method has also been used to obtain TiO_2 for evaluation in photocatalysis, among other applications [7,33–35], as this method can be easily used in the synthesis of core@shell systems, as described previously [36–38]. For instance, Mourão et al. [38] synthesized the core@shell system $CoFe_2O_4$@TiO_2 using the polymeric precursor method (derived from the Pechini method) for the synthesis of both materials and the photocatalysts were evaluated in the photodegradation of atrazine pesticide and RhB dye, with better results when high amounts of TiO_2 were use.

In the present work, the discoloration of a textile azo-dye using photocatalysis was evaluated because these compounds are widely used by textile industries, and their degradation is considered a difficult task [39,40]. A core@shell system was used as a photocatalyst, using a commercial nanometric (Co,Mn)Fe_2O_4 as the core and TiO_2 synthesized by the modified Pechini method as the shell. Synthesis parameters, such as the TiO_2 content, temperature and time of synthesis, were evaluated.

2. Materials and methods

Titanium resin was synthesized by the modified Pechini method using titanium isopropoxide (Sigma Aldrich, 97%), anhydrous citric acid (Cargill) and ethylene glycol (Vetec), with a metal:citric acid molar ratio of 1:3 and a citric acid: ethylene glycol mass ratio of 60:40. Detailed description of the methodology has already been presented in the literature [41,42]. A commercial ferrite, (Co,Mn)Fe_2O_4 (Nanum Tecnologia, Brazil), was used as core for the synthesis of the (Co,Mn)Fe_2O_4@TiO_2 systems, which was performed by addition of different stoichiometric amounts of the ferrite nanoparticles to the titanium polymeric resin under stirring at 90 °C, in order to obtain TiO_2 concentrations of 10, 20, 40, 60, 80, 90 and 95%, in mass. The suspension was heat treated at 300 °C for 1 h to obtain the powder precursor, which was deagglomerated at 270 mesh and heat treated between 400 and 700 °C under stagnated air atmosphere.

All materials were analyzed by X-ray diffraction (XRD) using an XRD – 6000 diffractometer from SHIMADZU, using Cu Kα radiation, in the range of 10–80°. The amount of anatase and rutile in the samples was determined using the Spurr and Myers method [43]. Chemical composition was determined by X-ray fluorescence using the Shimadzu XRF-1800 equipment, under Cu Kα radiation. The surface chemical composition was evaluated by X-ray photoelectron spectroscopy with a VG ESCA 3000 spectrometer, by collection of the spectra using MgKα radiation with an energy resolution of 0.8 eV, and using the peak assigned to C_{1s} as a reference for the energy calibration of other species. Samples were characterized by UV–vis spectroscopy using a UV-2550 spectrometer from SHIMADZU in the diffuse reflectance mode, for the calculation of the band gap by the Wood and Tauc method [44]. Infrared spectroscopy was also used to characterize the samples with an IRPrestige-21 spectrometer from SHIMADZU, using KBr pellets with 1% of sample. Scanning was performed between 400 and 4000 cm^{-1}, with 4 cm^{-1} of resolution and 20 accumulations. Raman spectra were obtained by a Via Renishaw spectrophotometer with an Ar laser (518 nm), 20 mW of power, and a Raman shift range between 50 and 1300 cm^{-1} at room temperature. Surface area determination was accomplished by the BET method from N_2 adsorption data, using the BELSORP-mini II equipment from BEL Japan, Inc. Magnetic properties were measured by a vibrating sample magnetometer – (VSM, Lake Shore, 7410 model) with all data acquired in pattern atmosphere and at room temperature. Morphology evaluation was accomplished by field emission scanning electronic microscopy using a FEG-VP microscope from Zeiss Supra 35. X-ray mapping was obtained using a Leo 1430 microscope at a voltage of 15 kV.

The photocatalytic tests concerning Remazol Golden Yellow azo dye (RNL) were performed in a Labmade reactor, with a low power UVC lamp (E = 4.9 eV or λ = 253 nm; P = 0.5–1 W measured near the sample). Petri dishes (5.5 cm in diameter and 1.5 cm in depth) with 10 mg of the catalyst and 15 mL of the RNL solution (10 mg L^{-1}) at pH 6 were positioned 5 cm from the lamp for 4, 8 and 16 h [45,46]. A blank solution was analyzed under the same conditions to evaluate the photolysis, which was calculated as 6.2% of discoloration after 16 h of UV irradiation. Discoloration of the methylene blue dye (MB) was also performed by photocatalytic tests, which were done in a magnetic stirred quartz reactor irradiated with three 9 W UVC OSRAM Puritec lamps with main emission at 254 nm, using 60 mg of catalyst and 90 mL of a 10 mg L^{-1} of MB aqueous solution. For this reactor, a photolysis of 6.5% was measured after 16 h of UV irradiation. For all of the tests, catalyst was removed with the aid of a magnet and the solution was evaluated by UV–vis spectroscopy with the same equipment described above, using the transmittance mode. Quantification of the discoloration (conversion) was done from a previously determined calibration curve, obtained from the intensity of the absorption band at 410 nm using solutions with known concentrations of the dye [47].

3. Results and discussion

3.1. (Co,Mn)Fe_2O_4@TiO_2 system with different amounts of TiO_2

Commercial ferrite was characterized by XRF and its composition was determined as $Co_{0.53}Mn_{0.31}Fe_{2.16}O_4$. In spite of the solid solution, XRD pattern (Fig. 1) indicated the presence of a single phase material with lattice parameter a = 8.43 Å. A BET surface area of 71 $m^2 g^{-1}$ was observed, equivalent to a particle size D_{BET} = 16 nm, which is similar to the values obtained by SEM (around 20 nm). According to literature [48,49], $CoFe_2O_4$ has a high Curie temperature ($T_c \approx 520$ °C) while $MnFe_2O_4$ has a smaller one ($T_c \approx 300$ °C), so that intermediate compositions should have intermediate transition temperatures – for instance Chougule et al [49] obtained T_c = 481 °C for $Co_{0.7}Mn_{0.3}Fe_2O_4$. In the present case, as photocatalytic reactions as well as catalyst separation are done at room temperature, this Curie temperature would not influence the separation process.

According to Fig. 1, peaks assigned to titanium dioxide are observed in the XRD patterns of the core@shell systems calcined at 700 °C when TiO_2 concentrations above 20% are used. The anatase and rutile phases are observed, with the main peaks at 25.3° (1 0 1) and 27.4° (1 1 0), respectively, in agreement to the ICDD index cards 71–1166 and 21–1276, with a higher amount of rutile especially for samples with higher TiO_2 concentration. The presence of hematite is indicated by the non-superposed high intensity peaks at 24.2, 33.2 and 49.3° assigned to the (0 1 2), (1 0 4) and (0 2 4) reflections, respectively, and it may also be observed for samples with TiO_2 concentration above 20%, and decreases as TiO_2 amount increases. The presence of Fe_2O_3 was also observed by Liu et al. [50,51] during the synthesis of $NiFe_2O_4$@TiO_2 samples by the sol-gel method, which was assigned to an impurity of the ferrite material. In the present case, as no Fe_2O_3 was observed in the commercial ferrite, its presence even when 90% of TiO_2 is used in the core-shell was assigned to Fe diffusion from ferrite. As a consequence, after synthesis of the core-shell material, lattice parameters of the ferrite had a random variation, with 'a' values between 8.36 and 8.41 Å.

UV–vis spectra are presented in Fig. 2. Similar to the XRD patterns, samples with a TiO_2 amount smaller than 40% have spectra with a profile similar to that of the ferrite sample. For samples with more than 40% TiO_2, an absorption band at 3.0 becomes evident, which is assigned to TiO_2. When the TiO_2 amount reaches 90%, a blueshift of the

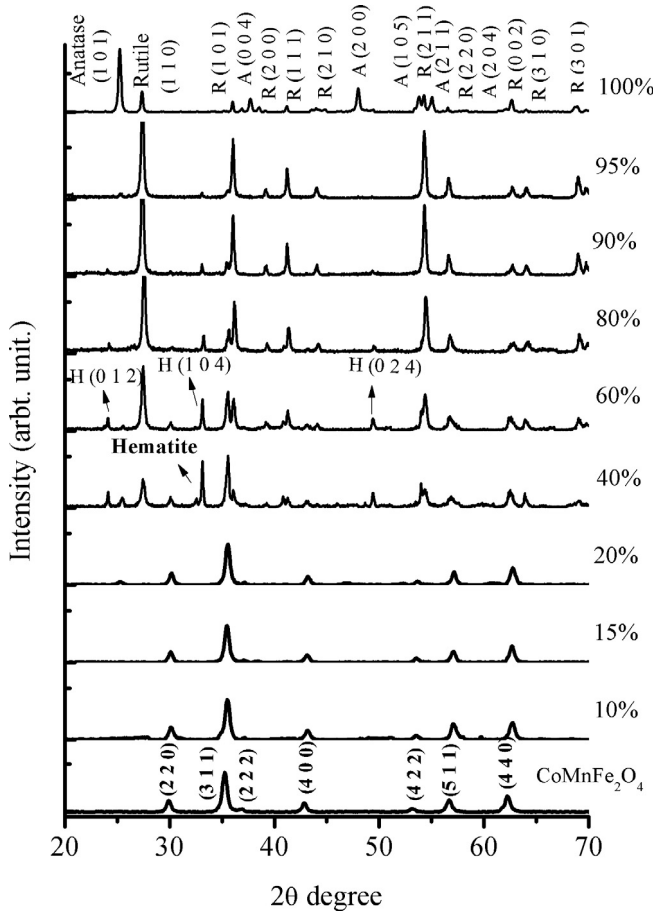

Fig. 1. XRD patterns of the materials synthesized with different amounts of titanium dioxide and heat treated at 700 °C.

TiO_2 band is observed and the spectrum becomes more similar to that of TiO_2, with absorptions below 2.5 eV, characteristic of the ferrite phase.

Magnetism analysis (Fig. 3) confirmed a decrease in magnetic properties as the amount of TiO_2 increased. Despite this result, all samples still presented magnetic saturation even when 95% TiO_2 was used. Magnetic performance analysis indicates the increase of shells with the same magnetic core strongly decreased the saturation magnetization, therefore reducing the efficiency in the magnetic separation process. The decrease of the saturation magnetization as TiO_2 amount increases was also observed by Liu et al. [50], who determined that this property is solely determined by the ferrite loading.

As expected, the increase of TiO_2 content decreased the surface area of the ferrites, as indicated by the specific surface area determinations with the BET method, described in Table 1. Despite this result, a high BET surface area in comparison to the pure TiO_2 one ($3.7\ m^2\ g^{-1}$) was attained and an initial increase in pore volume and pore diameter takes place followed by their decrease, which may be assigned to the sintering among TiO_2 particles. This change of morphology after TiO_2 deposition on ferrite can be observed by the FE-SEM micrographies displayed in Fig. 4. Ferrite particles are clearly agglomerated in pure samples, but after TiO_2 deposition a continuous matrix seems to involve the small particles, indicating an interaction among the ferrite particles and the polymeric resin.

Photocatalytic test results shown in Fig. 5a were realized using catalysts with different TiO_2 content, keeping the azo-dye concentration and the irradiation time constant. The samples with 20, 40 and 60% TiO_2 present photocatalytic efficiency similar to that of pure ferrite, whereas the sample with 80% TiO_2 presents intermediate efficiency. This behavior is probably related to the profile of the UV–vis spectra, which shows low energy transitions favoring recombination reactions. The highest conversions are attained for samples with higher amounts of TiO_2, 90% and 95%, which present UV–vis spectra with profiles more similar to that of TiO_2. The small activity may be related to the great amount of rutile phase. According to the literature data, synthesis methods that use lower temperatures, as with the solvothermal and liquid phase deposition route, lead to the formation of pure anatase in the shell for application in photocatalysis [24,26].

The magnetic properties for varying concentrations of TiO_2 are shown in Fig. 3-a and confirm that magnetism from the ferrite is maintained even when TiO_2 is deposited around it. Although the saturation field remained nearly constant, the saturation (Fig. 3-b) and the remnant magnetization (Fig. 3-d) followed a double exponential decay. Considering the best results of photocatalytic efficiency to guide magnetic measurements, the sample with 90% TiO_2 presented a $2.5\ emu\ g^{-1}$ for saturation magnetization with good efficiency in magnetic separation. For the 95% sample, even with the saturation magnetization being half that of the previous sample, its separation from an aqueous media was not possible.

For this reason, further tests were performed with the sample $(Co,Mn)Fe_2O_4@TiO_2$ 90%. FRX analysis of this sample confirmed the present of 88% of TiO_2, which indicated that a good stoichiometric control was attained. Even with 3% of the magnetic saturation obtained for the pure ferrite ($M_s = 83\ emu\ g^{-1}$), it was possible to separate this material from the aqueous solution using magnetism. This result is similar to the literature findings, which report that the high reduction of the magnetic saturation does not compromise its use for such applications [32].

3.2. $(Co,Mn)Fe_2O_4@TiO_2$ 90% system heat treated at different temperatures

It is well-known that materials with a mixture of anatase and rutile phases have higher photocatalytic efficiency than pure anatase [6]. For instance, P25 has an anatase:rutile phase ratio of 80:20. Moreover, during the Pechini method, materials are crystallized from an amorphous phase making it possible to obtain pure anatase (which is kinetically more stable), or a mixture of anatase and rutile phases with different ratios or pure rutile (which is thermodynamically more stable) [7,34].

As $(Co,Mn)Fe_2O_4@TiO_2$ 90% contains a large amount of the rutile phase, an evaluation of the calcination temperature was performed to optimize the anatase:rutile ratio. XRD patterns of samples calcined between 400 and 600 °C, displayed in Fig. 6, confirmed that samples with different anatase:rutile ratios were obtained. The phase amount was calculated according to the Spurr and Myers method [43] and indicated that the sample calcined at 400 °C presents a very low crystallinity, the samples calcined at 500 and 550 °C presented an anatase/rutile ratio similar to that of commercial P25, and the sample calcined at 600 °C has twice the amount of rutile phase as P25, besides peaks assigned to Fe_2O_3. The large amount of anatase phase in the samples calcined at 450, 500 and 550 °C was confirmed by Raman spectroscopy (Fig. S1 of the Supplementary Information). In relation to the ferrite, its presence is observed at lower calcination temperatures with a decrease of the peak intensity after calcination at 600 °C, when hematite is detected by a small intensity peak at 33.2°. For these samples, no meaningful change of the lattice parameter of the ferrite was detected with a values between 8.36 and 8.38 Å. Infrared spectra (Fig. S2 of the Supplementary Information) indicated that calcination was efficient in the elimination of organic material and that carbonate phases were not present.

UV–vis spectra are displayed in Fig. 7. All samples have band gap values smaller than that of pure TiO_2 (3.0 eV), making electronic recombination easier. For samples calcined at 450, 500 and 550 °C, a double band gap can be clearly observed. Absorbance below 2.5 eV may be assigned to the core material, in agreement with Fig. 2. This behavior may also be attributed to Fe^{3+}, as electronic transitions assigned to

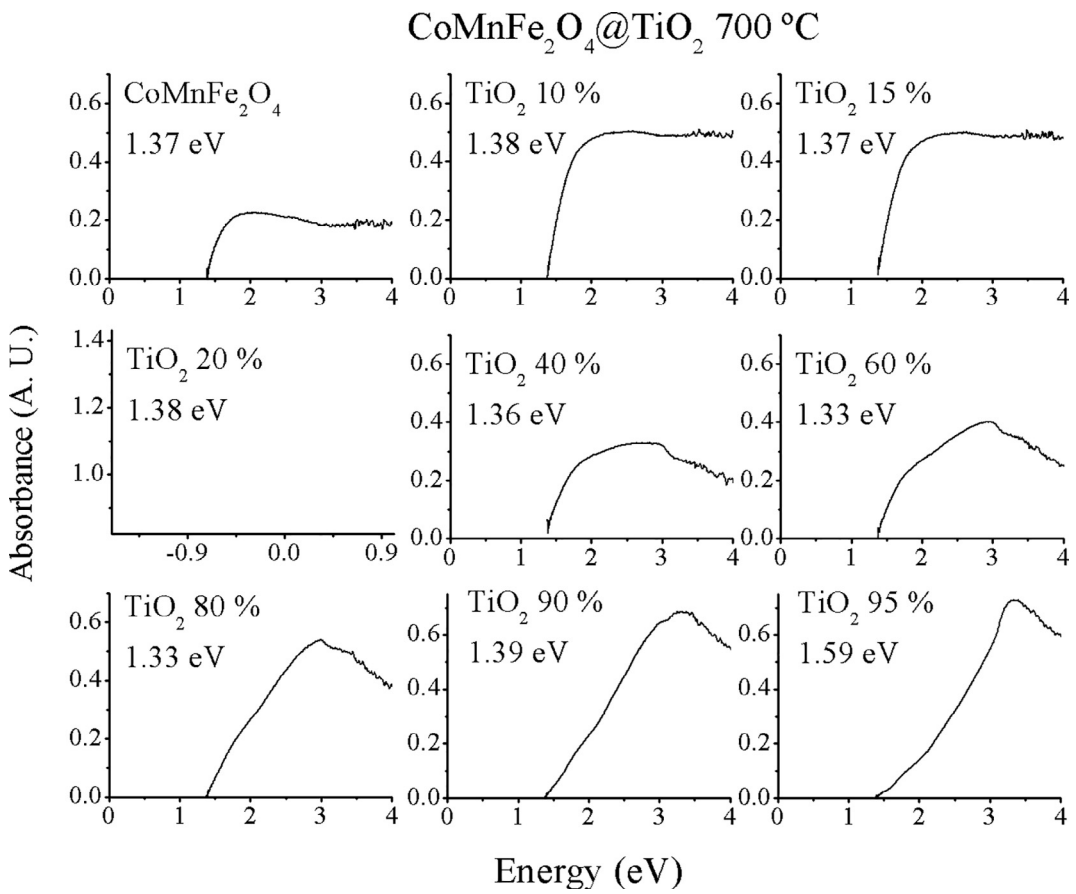

Fig. 2. UV–vis absorption spectra with the respective band gap energies of the materials synthesized with different amounts of TiO_2 and heat treated at 700 °C.

this cation are usually observed between 2.2 and 2.5 eV, besides transitions at 3.0 eV for Fe-doped TiO_2 [52]. Fe^{3+} may be present in the hematite phase in agreement with XRD patterns, or as an amorphous phase or even in the TiO_2 lattice.

Fig. 5b shows the results of photocatalytic tests performed using catalysts with 90% TiO_2 calcined between 450 and 600 °C, keeping the azo-dye concentration and the irradiation time constant. A meaningful decrease of the conversion with the heat treatment temperature was observed, which is assigned to the phase transition of TiO_2. Samples calcined at 450 and 500 °C, which presented a larger amount of anatase phase, also displayed the highest photocatalytic efficiency, whereas the sample calcined at 550 °C, which presented an anatase:rutile ratio similar to that of P25, presented a smaller efficiency. No clear correlation between conversion and band gap was noticed, as samples calcined at 500 and 550 °C had similar band gap values and different photocatalytic activities.

Direct comparison of the conversion values obtained in the present work with literature data may not be done, as different reaction conditions were used. For this reason, TiO_2 samples with anatase/rutile ratios similar to some samples obtained in the present work were synthesized by the same method and used in a photocatalytic reaction under the same conditions. When 96% of anatase was present in the TiO_2 sample, a conversion of 53% was obtained (2.3 fold higher the conversion obtained with the similar core@shell sample), while 64% of conversion was reached for a sample with 77% of anatase (4.3 fold higher). This meaningful difference may be related to the band gap, as the ferrite changed the profile of the UV–vis spectra of the ferrite@TiO_2 samples, with a meaningful decrease of the band gap, while the pure TiO_2 samples had a band gap value of 3.0 eV, with a step-like behavior.

The (Co,Mn)Fe_2O_4@TiO_2 90% sample calcined at 500 °C was evaluated by XPS, as presented in Fig. 8. Two high intensity peaks were observed, assigned to Ti $2p_{3/2}$ and O 1s, with binding energies of 461.8 and 533 eV, respectively (Fig. 8a). Ti $2p_{3/2}$ corresponds to the Ti^{4+} cation, whereas no peaks assigned to Ti^{3+} or Ti^{2+} were observed [53,54]. Similar results were obtained for the P25 sample and for TiO_2 obtained by the Pechini method, without ferrite addition. A decrease in the Ti-O bonding energy was observed in the core-shell (2.73 eV), compared to the pure TiO_2 calcined at 700 °C (3.0 eV).

The atomic concentration of the species on the sample surface was calculated from the integrated area of the respective peaks. The results indicated values of 21.8 and 73.5% for Ti $2p_{2/3}$ and O 1s, respectively, indicating that oxygen saturation occurs on the surface. One peak at 713 eV was also found, being assigned to $Fe_{2/3}$, leading to an atomic concentration of 1.7% (Fig. 8b). This atom may be present as a hematite phase or it may be incorporated into the TiO_2 lattice. Peaks assigned to cobalt or manganese were not observed, indicating that Fe ions migrated to the surface, while the spinel phase remained in the core of the material.

The formation of the TiO_2 shell around the ferrite was confirmed by X-ray mapping, as displayed in Fig. 9, obtained from a (Co,Mn) Fe_2O_4@TiO_2 90% sample calcined at 500 °C. Titanium is observed all around the particle, and an iron-rich particle is also noticed. These results indicate that iron oxide is formed due to iron migrating to the surface and reacting with oxygen, besides its incorporation into the TiO_2 lattice, as indicated by the superposition of the signals from Fe and Ti. Peaks assigned to cobalt or manganese were not observed. According to BET results, a surface area of 31 $m^2\,g^{-1}$ was attained for this sample.

Magnetic properties of several samples treated at different temperatures, shown in Fig. 10, were also evaluated. A step decrease of the magnetic saturation is observed between 500 and 550 °C, as displayed in Fig. 10b. According to Sharif et al [48], magnetic properties of

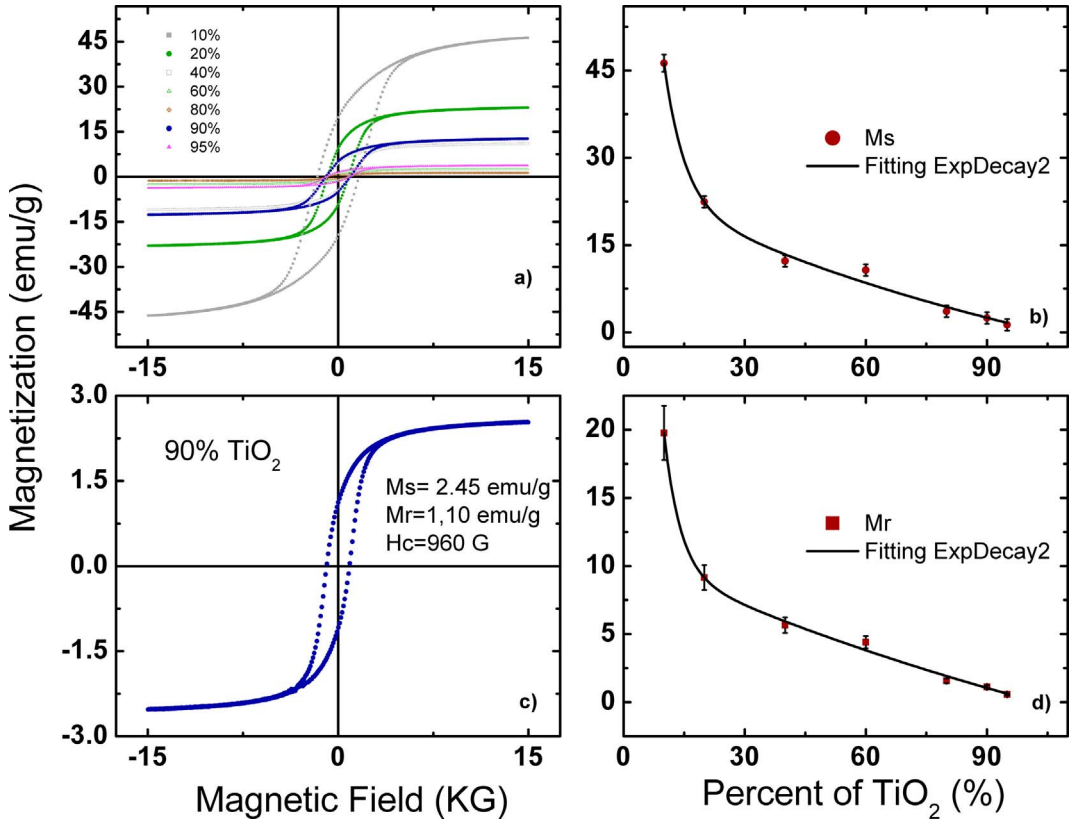

Fig. 3. Magnetic performance measurement at room temperature. a) Magnetization of the materials synthesized with different amounts of titanium dioxide and heat treated at 700 °C. b) Decrease of saturation magnetization (Ms) following a double exponential decay fit (gray line). c) Measurement for sample with 90% of TiO_2. d) Compilation of remanent magnetization (Mr.).

Table 1
Specific surface area obtained by the BET method.

Materials	$CoMnFe_2O_4$	10% 700 °C	15% 700 °C	20% 700 °C	90% 500 °C	TiO_2 700 °C
S_{BET} ($m^2 g^{-1}$)	73	62	50	52	31	4
V_m ($cm^3 g^{-1}$)	0.16	0.19	0.15	0.14	0.06	0.01
Pore diameter (nm)	9.2	11.7	11.2	10.2	8.4	13.6

nanomaterials are influenced by the particle size, formation of dead layer on the surface, random canting of particle surface spins, random particle size distribution, cation distribution in the spinel sites and presence of adsorbed water. When the particle size decreases the coercivity increases up to a single domain region and then decreases as a result of superparamagnetic size. Superparamagnetic and single domain diameters vary for different ferrites – for $CoFe_2O_4$ the single domain limit is around 40 nm [55]. In the present case, increase of the calcination temperature increased the crystallite size, as indicated in the Fig. S3 of the Supplementary information. For instance, between 500 and 550 °C, crystallite size increases from 51 to 61 nm, while saturation magnetization decreases from 5.7 emu g^{-1} to 2.5 emu g^{-1} and coercivity decreases from 1.9 to 0.7 kOe (Fig. S4 of the Supplementary Information), which may be assigned to a single domain transition.

Besides the higher conversions observed in the photocatalytic tests, another advantage of the decrease of the calcination temperature from 700 to 500 °C is the increase of the saturation magnetization from 2.5 emu g^{-1} to 5.7 emu g^{-1}, making the magnetic separation process easier. Furthermore, remnant magnetization for this sample allows the once magnetized material to be held together after the external field has been removed.

3.3. $(Co,Mn)Fe_2O_4@TiO_2$ 90% system heat treated at different times

Samples calcined at 450 and 500 °C were heat treated for longer periods (8 h) to improve the crystallinity and the rutile content (Fig. 11). These samples were chosen due to their higher photocatalytic activities, as reported in Fig. 5b. No meaningful change in the profile of the UV–vis spectra was observed after the increase in the heat treatment period, as showed in the Fig. S5 of the Supplementary information, indicating that the technique is not sensitive enough to detect these small changes. Moreover, no meaningful change in the magnetic saturation was observed, as indicated in Fig. S4 of the Supplementary Information.

Photocatalytic tests were performed under the same conditions described before, as displayed in Fig. 5c and in Fig. S6 of the Supplementary informations. A meaningful improvement was observed for both photocatalysts, with a 27% increase in discoloration for the sample calcined at 450 °C for 8 h and a 47% increase for the sample calcined at 500 °C for 8 h. This last sample was also used during tests with 8 and 16 h of UV irradiation, reaching 76.3% discoloration after the longest exposure time, which was the highest conversion obtained in the present work. The UV–vis absorption curves are displayed in the Supplementary Informations for the sample $(Co,Mn)Fe_2O_4@TiO_2$ 90% 500 °C/8 h, using different irradiation times. An adsorption test was performed for this sample, with a contact period of 16 h in dark conditions, but no discoloration was observed, which confirms that a photocatalytic reaction had occurred. The absence of adsorption indicates that an indirect photocatalytic mechanism takes place in the present case. According to literature [56], hydroxyl radicals seem to be the major reactive species at neutral or high pH levels.

A smaller photocatalytic efficiency was attained, compared to that of P25. This behavior may be attributed to the small band gap energy, which makes electron/hole recombination easier. The presence of iron

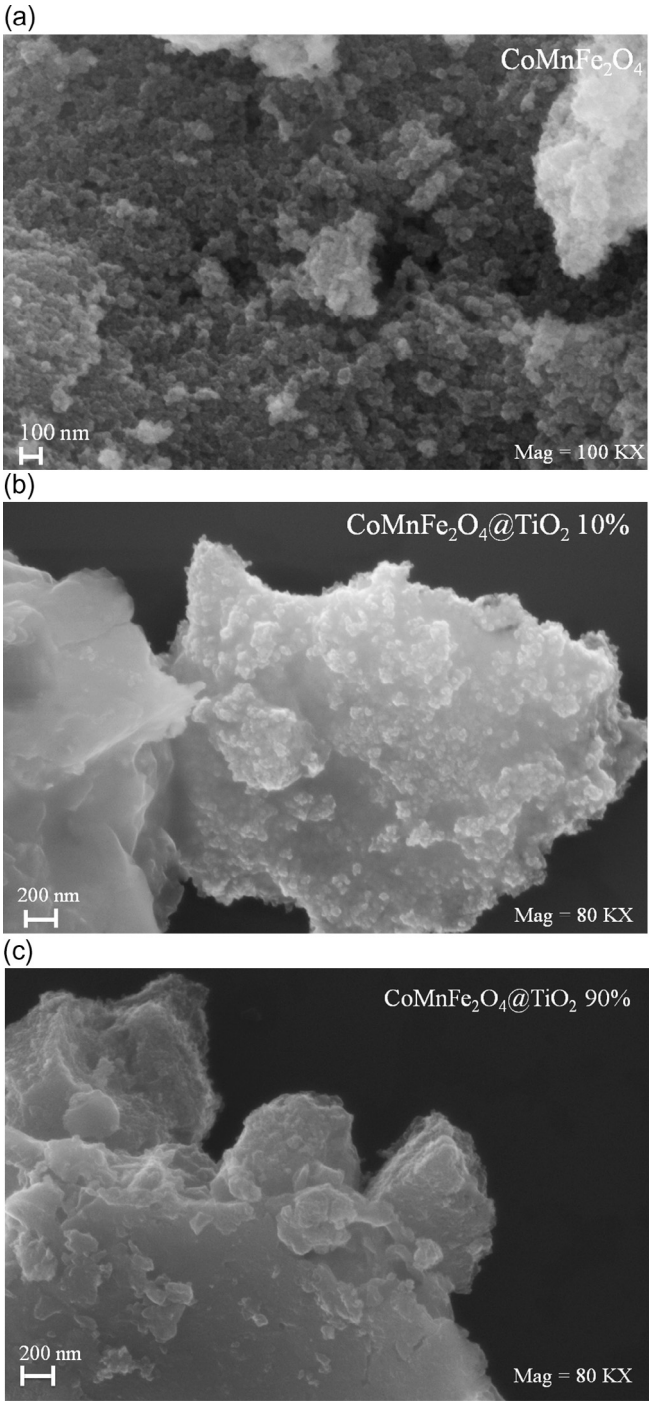

Fig. 4. FE-SEM micrographies of the pure (Co,Mn)Fe_2O_4 sample (a) and of the (Co,Mn) Fe_2O_4@TiO_2 systems with 10% (b) and 90% (c) of TiO_2.

oxide may also decrease the efficiency as electrons may be transferred to the transition metal, leading to redox reactions. In both cases, recombination or redox reactions, electrons become less available to the formation of hydroxyl radicals. Moreover, the surface area of P25 (50 $m^2 g^{-1}$) is greater than that of (Co,Mn)Fe_2O_4@TiO_2 90% 500 °C.

Harraz et al. [27] also detected Fe and Co on the surface of the titania-silica/cobalt ferrite nanocomposite by XPS analysis, but the authors obtained a high photocatalytic efficiency, which may be attributed to the large surface area and to the use a high-power UV lamp (150 W). A large degree of photocatalytic degradation of methylene blue was also obtained by Wu et al. [29] using magnetic iron oxides/TiO_2 and a high power UV lamp (250 W) and by Zheng et al. [26] using

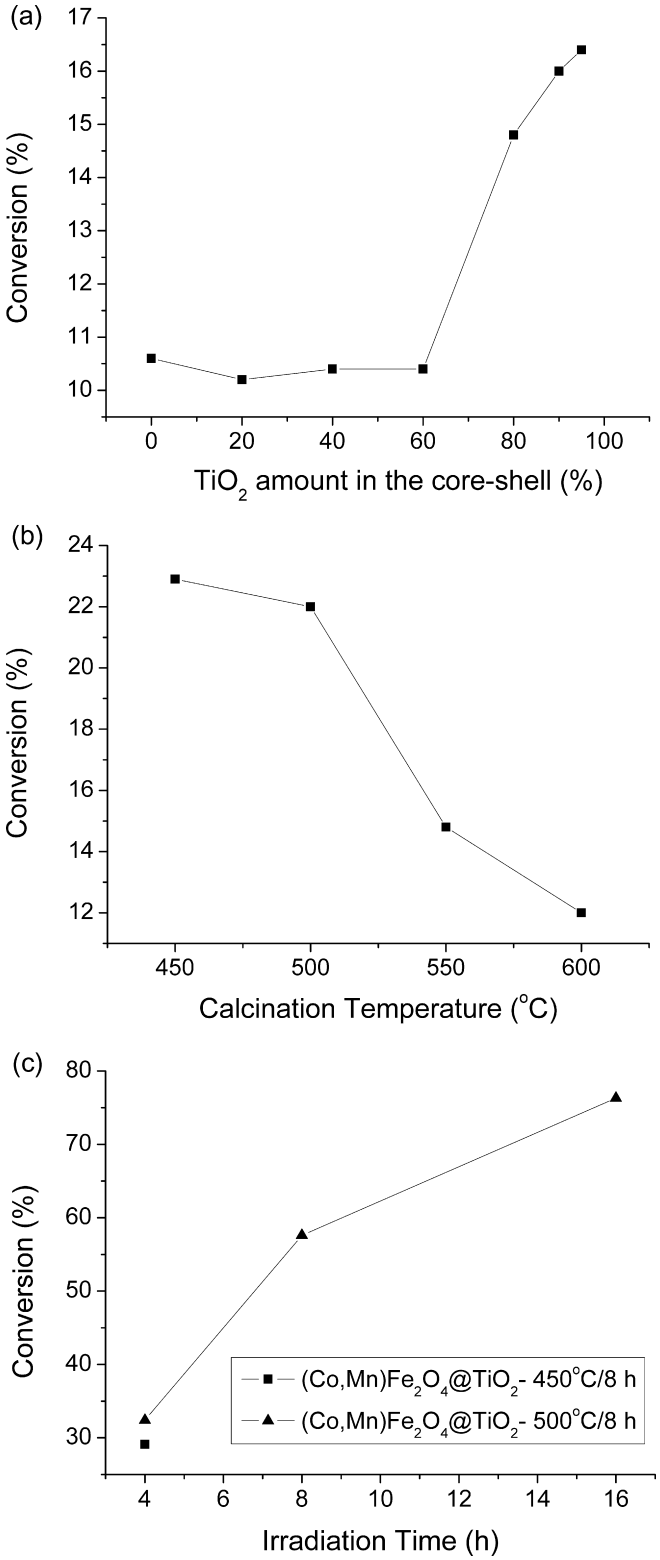

Fig. 5. Results of the conversions obtained during photocatalytic tests performed with 10 mg of the catalyst and 15 mL of the RNL solution (10 mg L^{-1}) at pH 6, at room temperature. (a) Photocatalytic test for a period of 4 h using catalysts with different TiO_2 amounts, heat treated at 700 °C for 4 h; (b) Photocatalytic test for a period of 4 h using catalysts with 90% of TiO_2 heat treated at different temperatures for 4 h; (c) Photocatalytic test for different periods of time using catalysts with 90% of TiO_2 heat treated at 450 or 500 °C for 8 h.

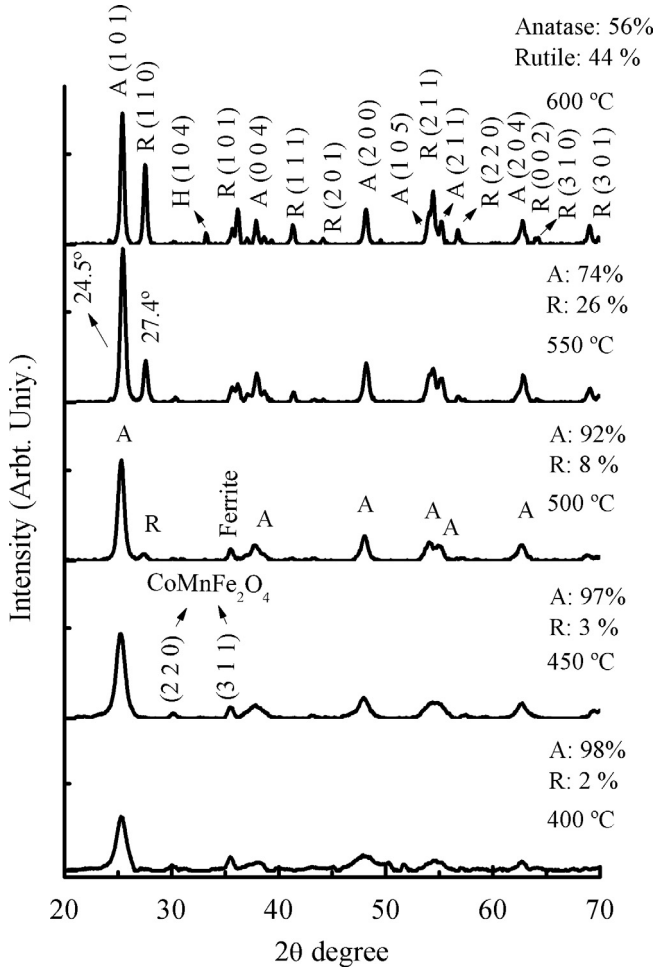

Fig. 6. XRD patterns of the core@shell systems synthesized with 90% of titanium dioxide and heat treated at different temperatures.

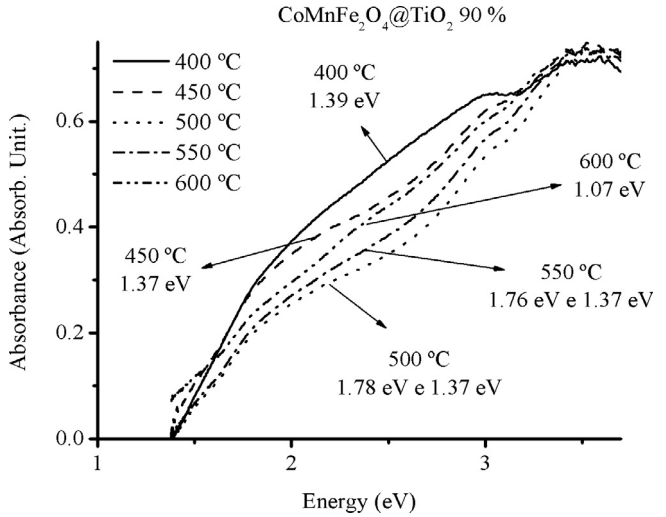

Fig. 7. UV–vis absorption spectra of the core@shell systems synthesized with 90% of titanium dioxide and heat treated at different temperatures.

Fe_3O_4@TiO_2, using visible irradiation from a xenonium lamp of 300 W. Despite the good results, conversion determined by Zheng et al. was less than that of the commercial P25 TiO_2, probably due to the different physico-chemical properties of the two materials.

For comparison with literature data, the most efficient photocatalyst obtained in the present work was used in the photodegradation of

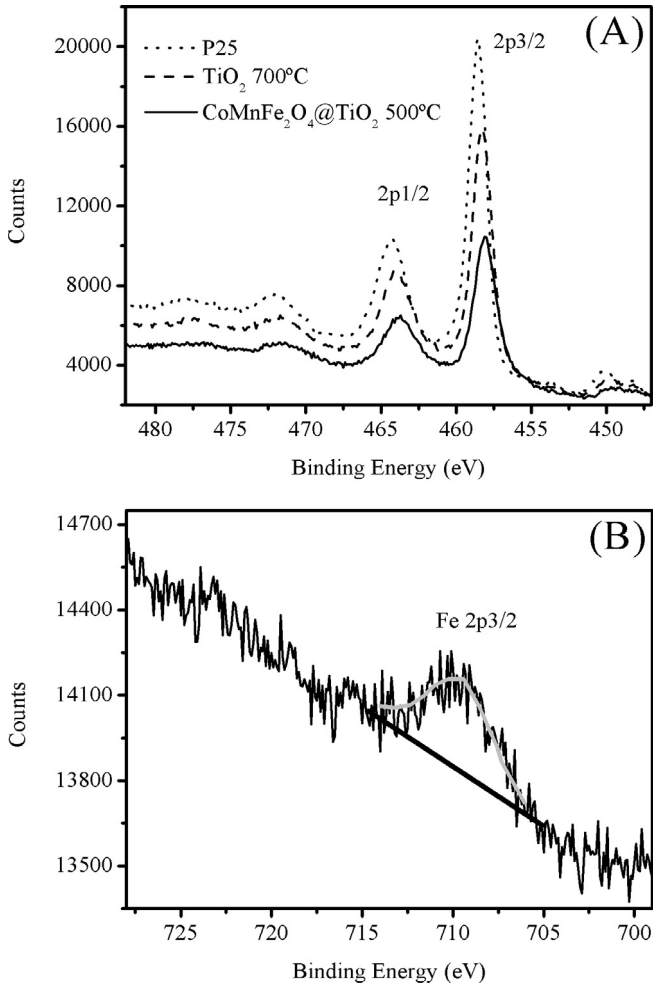

Fig. 8. XPS spectra of the sample (Co,Mn)Fe_2O_4@TiO_2 90% heat treated at 500 °C, compared to the P25 one and to the TiO_2 obtained by the modified Pechini method (a) Detail showing the Ti2p signal in all of the samples; (b) Peak assigned to Fe 2p in the core@shell sample.

methylene blue, as presented in Fig. S7 of the Supplementary information. A conversion of 49% of attained after 16 h of UVC irradiation, while 48% of conversion was attained during reuse. Adsorption showed a discoloration of 14.9% indicating that a direct mechanism may also be present during photocatalytic reaction. This conversion may not be compared to the RNL one because different reactors were used. The smallest conversion obtained in the present work in comparison to literature data may be assigned to the use of a much less powerful lamp.

4. Conclusions

Results obtained in the present work indicated that the (Co,Mn)Fe_2O_4@TiO_2 system may be used as a photocatalyst for RNL discoloration with an easy withdrawal from the reaction media. The increase in the amount of TiO_2 used in the system improved the photocatalytic efficiency and did not cancel the magnetic property of the ferrite up to 90% TiO_2 content. A meaningful influence of the heat treatment temperature in the photocatalytic efficiency was observed, being assigned to the anatase – rutile phase transition. XPS and X-ray mapping did not show the presence of cobalt or manganese near the surface, indicating that a core@shell system was obtained. Despite this result, iron was clearly observed indicating that it migrated from the spinel phase to the surface, which probably resulted in the smaller photocatalytic efficiency. A discoloration of 76.3% was attained after

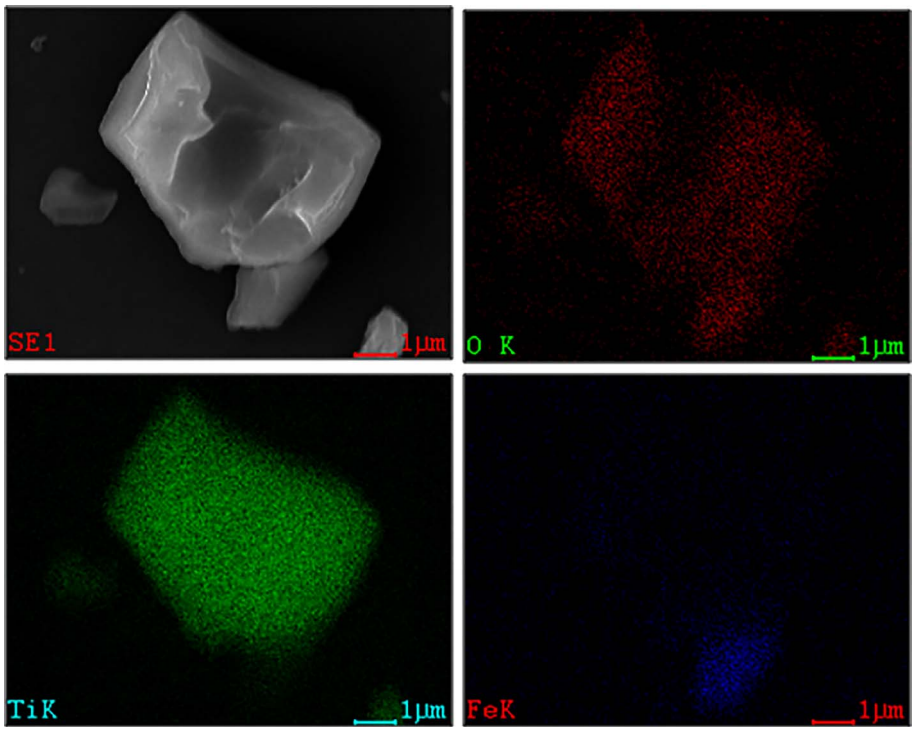

Fig. 9. X-ray mapping of the sample (Co,Mn)Fe_2O_4@TiO_2 90% heat treated at 500 °C.

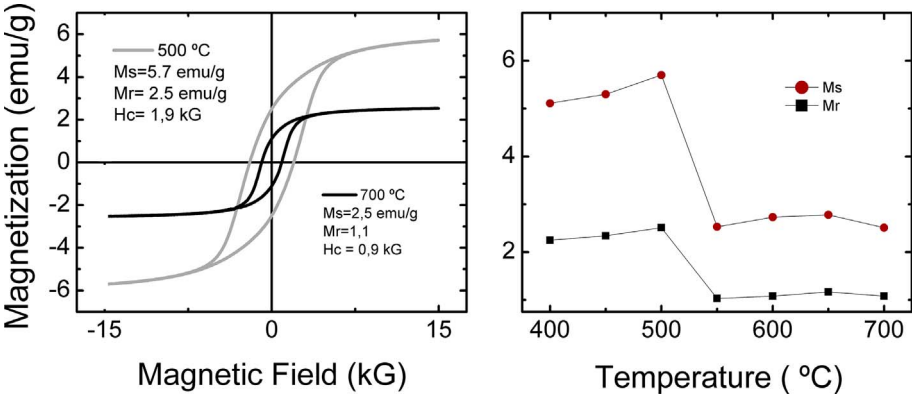

Fig. 10. a) Magnetization of the sample (Co,Mn)Fe_2O_4@TiO_2 90% heat treated at 500 °C and 700 °C. b) Analysis of saturation and remanent magnetizations for several samples treated at different temperatures. All measurements were performed at room temperature.

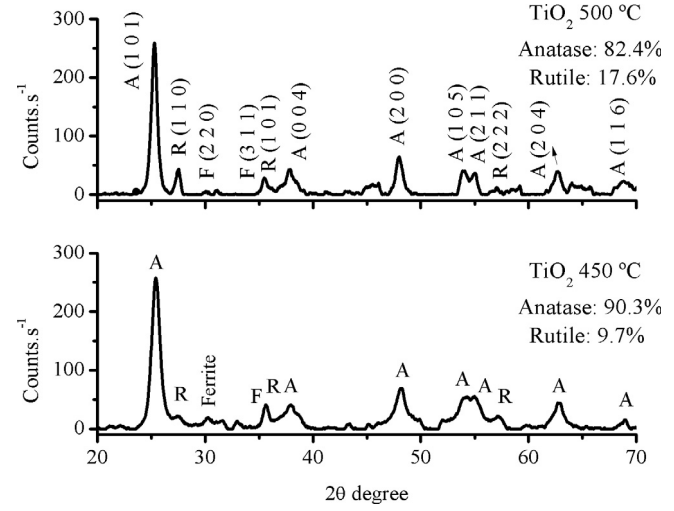

Fig. 11. XRD patterns of the samples containing 90% of TiO_2 heat treated at 450 or 500 °C for 8 h.

16 h of UV irradiation using the system (Co,Mn)Fe_2O_4@TiO_2 90%, calcined at 500 °C for 8 h.

Acknowledgements

This work was supported by Brazilian Funding Agencies CT-INFRA/FINEP/MCTIC, CAPES/MEC, FAPERN and FAPESP. The authors are grateful to Nanum, who kindly supplied the nanometric ferrite sample.

Appendix A. Supplementary data

Supplementary data associated with this article can be found, in the online version, at http://dx.doi.org/10.1016/j.mseb.2017.12.029.

References

[1] F.C. Moreira, R.A.R. Boaventura, E. Brillas, V.J.P. Vilar, Electrochemical advanced oxidation processes: a review on their application to synthetic and real wastewaters, Appl. Catal., B 202 (2017) 217–261.
[2] G. Boczkaj, A. Fernandes, Wastewater treatment by means of advanced oxidation processes at basic pH conditions: a review, Chem. Eng. J. 320 (2017) 608–633.
[3] R. Dewil, D. Mantzavinow, I. Poulios, M.A. Rodrigo, New perspectives for advanced oxidation processes, J. Environ. Manage. 195 (2017) 93–99.
[4] H. Suzuki, S. Araki, H. Yamamoto, Evaluation of advanced oxidation processes

(AOP) using O_3 UV and TiO_2 for the degradation of phenol in water, J. Water Process Eng. 7 (2015) 54–60.
[5] J. Moellmann, S. Ehrlich, R. Tonner, S. Grimme, A DFT-D study of structural and energetic properties of TiO_2 modifications, J. Phys.: Condens. Matter 24 (2012) 424206 (8pp).
[6] D.O. Scanlon, C.W. Dunnill, J. Buckeridge, S.A. Shevlin, A.J. Logsdail, S.M. Woodley, C.R.A. Catlow, M.J. Powell, R.G. Palgrave, I.P. Parkin, G.W. Watson, T.W. Keal, P. Sherwood, A. Walsh, A.A. Sokol, Band alignment of rutile and anatase TiO_2, Nat. Mater. 12 (2013) 798–801.
[7] M.P.F. Graça, C. Nico, M. Peres, M.A. Valente, T. Monteiro, Study of the optical and dielectric properties of TiO_2 nanocrystals prepared by the Pechini Method, J. Nanosci. Nanotechnol. 12 (2012) 8600–8606.
[8] S.G. Kumar, L.G. Devi, Review on modified TiO_2 photocatalysis under UV/Visible light: selected results and related mechanisms on interfacial charge carrier transfer dynamics, J. Phys. Chem. A 115 (2011) 13211–13241.
[9] K. Nakata, A. Fujishima, TiO_2 photocatalysis: design and applications, J. Photochem. Photobiol., C 13 (2012) 169–184.
[10] M.A. Rauf, M.A. Meetani, S. Hisaindee, An overview on the photocatalytic degradation of azo dyes in the presence of TiO_2 doped with selective transition metals, Desalination 276 (2011) 13–27.
[11] D.F.M. Oliveira, P.S. Batista, P.S. Muller Jr., V. Velani, M.D. França, D.R. Souza, A.E.H. Machado, Evaluating the effectiveness of photocatalysts based on titanium dioxide in the degradation of the dye Ponceau 4R, Dyes Pigm. 92 (2011) 563–572.
[12] M. Rani, U. Shanker, V. Jassal, Recent strategies for removal and degradation of persistent & toxic organochlorine pesticides using nanoparticles: a review, J. Environ. Manage. 190 (2017) 208–222.
[13] P.V.L. Reddy, B. Kavitha, P.A.K. Reddy, K.H. Kim, TiO_2-based photocatalytic disinfection of microbes in aqueous media: a review, Environ. Res. 154 (2017) 296–303.
[14] R. Fagan, D.E. McCormack, D.D. Dionysiou, S.C. Pillai, A review of solar and visible light active TiO_2 photocatalysis for treating bacteria, cyanotoxins and contaminants of emerging concern, Mater. Sci. Semicond. Process. 42 (2016) 2–14.
[15] K.H. Leong, P. Monash, S. Ibrahim, P. Saravanan, Solar photocatalytic activity of anatase TiO_2 nanocrystals synthesized by non-hydrolitic sol-gel method, Sol. Energy 101 (2014) 321–332.
[16] R. Velmurugan, B. Krishnakumar, B. Subash, M. Swaminathan, Preparation and characterization of carbon nanoparticles loaded TiO_2 and its catalytic activity driven by natural sunlight, Sol. Energy Mater. Sol. Cells 108 (2013) 205–212.
[17] A.O. Kondrakov, A.N. Ignatev, F.H. Frimmel, S. Bräse, H. Horn, A.I. Revelsky, Formation of genotoxic quinones during bisphenol A degradation by TiO_2 photocatalysis and UV photolysis: a comparative study, Appl. Catal., B 160 (2014) 106–114.
[18] F. Oshani, R. Marandi, S. Rasouli, M.K. Farhoud, Photocatalytic investigations of TiO_2–P25 nanocomposite thin films prepared by peroxotitanic acid modified sol-gel method, Appl. Surf. Sci. 311 (2014) 308–313.
[19] J. Gómez-Pastora, S. Dominguez, E. Bringas, M.J. Rivero, I. Ortiz, D.D. Dionysiou, Review and perspectives on the use of magnetic nanophotocatalysts (MNPCs) in water treatment, Chem. Eng. J. 310 (2017) 407–427.
[20] M.A. Habila, Z.A. Alothoman, A.M. El-Toni, J.P. Labis, M. Soylak, Synthesis and application of Fe_3O_4@SiO_2@TiO_2 for photocatalytic decomposition of organic matrix simultaneously with magnetic solid phase extraction of heavy metals prior to ICP-MS analysis, Talanta 154 (2016) 539–547.
[21] M. Wilson, C.Y.C. Cheng, G. Oswald, R. Srivastava, S.K. Beaumont, J.P.S. Badyal, Magnetic recyclable microcomposite silica-steel core with TiO_2 nanocomposite shell photocatalysts for sustainable water purification, Colloids Surf., A 523 (2017) 27–37.
[22] M.B. Gawande, A. Goswami, T. Asefa, H. Guo, A.V. Biradar, D.-L. Peng, R. Zboril, R.S. Varma, Core-shell nanoparticle: synthesis and applications in catalysis and electrocatalysis, Chem. Soc. Rev. 44 (2015) 7540–7590.
[23] A.M. El-Toni, M.A. Habila, J.P. Labis, Z.A. ALOthman, M. Alhoshan, A.A. Elzatahry, F. Zhang, Design, synthesis and applications of core-shell hollow core, and nanorattle multifunctional nanostructures, Nanoscale 8 (2016) 2510–2531.
[24] T. Xin, M. Ma, H. Zhang, J. Gu, S. Wang, M. Liu, Q. Zhang, A facile approach for the synthesis of magnetic separable Fe_3O_4@TiO_2, core-shell nanocomposites as highly recyclable photocatalysts, Appl. Surf. Sci. 288 (2014) 51–59.
[25] K.-H. Choi, S.-Y. Park, B.J. Park, J.-S. Jung, Recyclable Ag-coated Fe_3O_4@TiO_2 for efficient photocatalytic oxidation of chlorophenol, Surf. Coat. Technol. 320 (2017) 240–245.
[26] J. Zheng, Y. Wu, Q. Zhang, Y. Li, C. Wang, Y. Zhou, Direct liquid phase deposition fabrication of waxberry-like magnetic Fe_3O_4@TiO_2 core-shell microspheres, Mater. Chem. Phys. 181 (2016) 391–396.
[27] F.A. Harraz, R.M. Mohamed, M.M. Rashad, Y.C. Wang, W. Sigmund, Magnetic nanocomposite based on titania-silica/cobalt ferrite for photocatalytic degradation of methylene blue dye, Ceram. Int. 40 (2014) 375–384.
[28] A. Wilson, S.R. Mishra, R. Gupta, K. Ghosh, Preparation and photocatalytic properties of hybrid core-shell reusable $CoFe_2O_4$@ZnO nanospheres, J. Magn. Magn. Mater. 324 (2012) 2597–2601.
[29] W. Wu, X. Xiao, S. Zhang, F. Ren, C. Jiang, Facile method to synthesize magnetic iron oxides/TiO_2 hybrid nanoparticles and their photodegradation application of methylene blue, Nanoscale Res. Lett. 6 (2011) 533–548.
[30] B. Tian, T. Wang, R. Dong, S. Bao, F. Yang, J. Zhang, Core-shell structured γ-Fe_3O_4@SiO_2@AgBr: Ag composite with high magnetic separation efficiency and excellent visible light activity for acid orange 7 degradation, Appl. Catal., B 147 (2014) 22–28.
[31] L. Gan, L. Xu, K. Qian, Preparation of core-she structured $CoFe_2O_4$ incorporated Ag_3PO_4 nanocomposites for photocatalytic degradation of organic dyes, Mater. Des. 109 (2016) 354–360.
[32] Y.-F. Zhang, L.-G. Qiu, Y.-P. Yuan, Y.-J. Zhu, X. Jiang, J.-D. Xiao, Magnetic Fe_3O_4@C/Cu and Fe_3O_4@CuO core-shell composites constructed from MOF-based materials and their photocatalytic properties under visible light, Appl. Catal., B 144 (2014) 863–869.
[33] R.G. Chaudhuri, S. Paria, Core/shell nanoparticles: classes properties, synthesis mechanisms, characterization and applications, Chem. Rev. 112 (2012) 2373–2433.
[34] P.C. Ribeiro, A.C.F.M. Costa, R.H.G.A. Kiminami, J.M. Sasaki, H.L. Lira, Synthesis of TiO_2 by the Pechini method and photocatalytic degradation of methyl red, Mater. Res. 16 (2013) 468–472.
[35] A. Mashreghi, M. Ghasemi, Investigating the effect of molar ratio between TiO_2 nanoparticles and titanium alkoxide in Pechini based TiO_2 paste on photovoltaic performance of dye-sensitized solar cells, Renew. Energy 75 (2015) 481–488.
[36] M.P. Pechini, Method of preparing lead and alkaline earth titanates and niobates and coating method using the same to form a capacitor, Patent U.S. 3330697, (1967).
[37] G.L. Lucena, A.S. Maia, E. Longo, A.G. Souza, I.M.G. Santos, A facile synthesis method to obtain $SrSnO_3$@AO_2 (A = Ti or Zr) core shell systems, Curr. Phys. Chem. 5 (2016) 214–222.
[38] H.A.J.L. Mourão, A.R. Malagutti, C. Ribeiro, Synthesis of TiO_2-coated $CoFe_2O_4$ photocatalysts applied to the photodegradation of atrazine and rhodamine B in water, Appl. Catal., A 382 (2010) 284–292.
[39] M.F. Akhtar, M. Ashraf, A.A. Anjum, A. Javeed, A. Sharif, A. Saleem, B. Akhtar, Textile industrial effluent induces mutagenicity and oxidative DNA damage and exploits oxidative stress biomarkers in rats, Environ. Toxicol. Pharmacol. 41 (2016) 180–186.
[40] L.R. Martins, B.E.L. Baêta, L.V.A. Gurgel, S.F. Aquino, L.F. Gil, Application of cellulose-immobilized riboflavin as a redox mediator for anaerobic degradation of a model azo dye Remazol Golden Yellow RNL, Ind. Crops Prod. 65 (2015) 454–462.
[41] S.C. Souza, M.A.F. Souza, S.J.G. Lima, M.R. Cassia-Santos, V.J. Fernandes Jr., L.E.B. Soledade, E. Longo, A.G. Souza, I.M.G. Santos, The effects of co, ni and mn on the thermal processing of Zn_2TiO_4 pigments, J. Therm. Anal. Calorim. 79 (2005) 455–459.
[42] S.C. Souza, I.M.G. Santos, M.R.S. Silva, M.R. Cássia-Santos, L.E.B. Soledade, A.G. Souza, S.J.G. Lima, E. Longo, Influence of pH on iron doped Zn_2TiO_4 pigments, J. Therm. Anal. Calorim. 79 (2005) 451–454.
[43] R.A. Spurr, H. Myres, Quantitative analysis of anatase-rutile mixtures with an x-ray diffractometer, Anal. Chem. 29 (1957) 760–762.
[44] D.L. Wood, J. Tauc, Weak absorption tails in amorphous semiconductors, Phys. Rev. B 5 (1972) 3144–3151.
[45] K.F. Moura, J. Maul, A.R. Albuquerque, G.P. Casali, E. Longo, D. Keyson, A.G. Souza, J.R. Sambrano, I.M.G. Santos, TiO_2 synthesized by microwave assisted solvothermal method: experimental and theoretical evaluation, J. Solid State Chem. 210 (2014) 171–177.
[46] J.M. Alvarenga, R.A. Fideles, M.V. Silva, G.F. Murari, J.G. Taylor, L.R. Lemos, G.D. Rodrigues, Partition study of textile dye Remazol Yellow Gold RNL in aqueous two-phase systems, Fluid Phase Equilib. 391 (2015) 1–8.
[47] H.B. Sales, V. Bouquet, S. Députier, S. Ollivier, F. Gouttefangeas, M. Guilloux-Viry, V. Dorcet, I.T. Weber, A.G. Souza, I.M.G. Santos, $Sr_{1-x}Ba_xSnO_3$ system applied in the photocatalytic discoloration of an azo-dye, Solid State Sci. 28 (2014) 67–73.
[48] I. Sharifi, H. Shokrollahi, S. Amiri, Ferrite-based magnetic nanofluids used in hyperthermia applications, J. Magn. Magn. Mater. 324 (2012) 903–915.
[49] P.K. Chougule, S.S. Kumbhar, Y.D. Kolekar, C.H. Bhosale, Enhancement in Curie temperature of nickel substituted Co-Mn ferrite, J. Magn. Magn. Mater. 372 (2014) 181–186.
[50] Y. Liu, P. Gao, N. Cherkasov, E.V. Rebrov, Direct amide synthesis over core-shell TiO_2@$NiFe_2O_4$ catalysts in a continuous flow radiofrequency-heated reactor, RSC Adv. 6 (2016) 100997.
[51] Y. Liu, N. Cherkasov, P. Gao, J. Fernández, M.R. Lees, E.V. Rebrov, The enhancement of direct amide synthesis reaction rate over TiO_2@SiO_2@$NiFe_2O_4$ magnetic catalysts in the continuous flow under radiofrequency heating, J. Catal. 355 (2017) 120–130.
[52] C. Fàbrega, T. Andreu, A. Cabot, J.R. Morante, Location and catalytic role of iron species in TiO_2: Fe photocatalysts: an EPR study, J. Photochem. Photobiol., A 211 (2010) 170–175.
[53] F. Liu, L. Lu, P. Xiao, H. He, L. Qiao, Y. Zhang, Effect of oxygen vacancies on photocatalytic efficiency of TiO_2 nanotubes aggregation, Bull. Korean Chem. Soc. 33 (2012) 2255–2259.
[54] R. Zanoni, G. Righini, A. Montenero, G. Gnappi, G. Montesperelli, E. Traversa, G. Gusmano, XPS analysis of sol-gel prossed doped and undoped TiO_2 films for sensors, Surf. Interface Anal. 22 (1994) 376–379.
[55] S. Singh, N. Khare, Defects/strain influenced magnetic properties and inverse of surface spin canting effect in single domain $CoFe_2O_4$ nanoparticles, Appl. Surf. Sci. 364 (2016) 783–788.
[56] I.K. Konstantinou, T.A. Albanis, TiO_2-assisted photocatalytic degradation of azo dyes in aqueous solution: kinetic and mechanistic investigations. A review, Appl. Catal. B 49 (2004) 1–14.